



Research Paper

HO-1-mediated ferroptosis as a target for protection against retinal pigment epithelium degeneration

Zhimin Tang¹, Yahan Ju¹, Xiaochan Dai¹, Ni Ni, Yan Liu, Dandan Zhang, Huiqin Gao, Hao Sun, Jing Zhang^{**}, Ping Gu^{*}

Department of Ophthalmology, Shanghai Ninth People's Hospital, Shanghai Jiao Tong University School of Medicine, Shanghai Key Laboratory of Orbital Diseases and Ocular Oncology, Shanghai, 200011, PR China



ARTICLE INFO

Keywords:

Ferroptosis
Heme oxygenase-1
Iron chelation
Retinal pigment epithelium
Age-related macular degeneration
Photoreceptor

ABSTRACT

Oxidative stress-mediated retinal pigment epithelium (RPE) degeneration plays a vital role in retinal degeneration with irreversible visual impairment, most notably in age-related macular degeneration (AMD), but a key pathogenic factor and the targeted medical control remain controversial and unclear. In this work, by sophisticated high-throughput sequencing and biochemistry investigations, the major pathologic processes during RPE degeneration in the sodium iodate-induced oxidative stress model has been identified to be heme oxygenase-1 (HO-1)-regulated ferroptosis, which is controlled by the Nrf2–SLC7A11–HO-1 hierarchy, through which ferrous ion accumulation and lethal oxidative stress cause RPE death and subsequently photoreceptor degeneration. By direct knockdown of HO-1 or using HO-1 inhibitor ZnPP, the specific inhibition of HO-1 overexpression has been determined to significantly block RPE ferroptosis. In mice, treatment with ZnPP effectively rescued RPE degeneration and achieved superior therapeutic effects: substantial recovery of the retinal structure and visual function. These findings highlight that targeting HO-1-mediated RPE ferroptosis could serve as an effectively retinal-protective strategy for retinal degenerative diseases prevention, including AMD.

1. Introduction

Monolayer retinal pigment epithelium (RPE) cells are located in an oxygen-rich retinal environment, which are vital to support the survival and biological function of overlying photoreceptors by performing multiple functions, including phagocytosis of photoreceptor outer segment tips, transepithelial transport of fluids and nutrients between choroid capillaries and photoreceptors, formation of outer blood–retinal barrier, and recycling of bleached visual pigment [1]. RPE failure in playing these roles could result in vision-threatening and even blinding conditions, particularly in age-related macular degeneration (AMD) [2, 3]. Presently, AMD is one of the most common eye diseases in clinic, and is estimated to affect about 288 million people in western countries by 2040 [4]. Although the explicit etiology of AMD is not thoroughly clear, it is widely acceptable that oxidative stress exerts a primary, causative effect on the increased susceptibility of metabolically active RPE cell death and subsequent photoreceptor degeneration, leading to the

ultimate loss of central vision. Iron, is a source of free radicals, and has been demonstrated in AMD pathogenesis [5]. It has been reported that excessive iron release after intraocular hemorrhage could induce peroxidation of unsaturated phospholipids and retinal inflammation [6,7]. These findings support the hypothesis that oxidative stress and iron toxicity are implicated in RPE cell dysfunction and the progression of AMD. However, the mechanisms underlying oxidative stress-mediated RPE cell death have not yet been completely understood. Previous studies employing exogenous pro-oxidants, *e.g.*, hydrogen peroxide (H₂O₂) and *tert*-butyl hydroperoxide (tBH), to culture RPE cells emphasized the role of deleterious oxidative stress in various cell death modes of RPE, including apoptosis, necrosis, necroptosis, and autophagy [8–11]. However, several degenerating processes cannot be explained by these pathogeneses and accordingly targeting drugs are limitedly effective. A novel type of programmed cell death, ferroptosis, has been demonstrated in neurodegenerative disease, *e.g.*, Alzheimer's disease and Parkinson's disease, which is inextricably associated with lipid

* Corresponding author.

** Corresponding author.

E-mail addresses: zhjingty@126.com (J. Zhang), guping2009@sjtu.edu.cn, guping2009@126.com (P. Gu).

¹ These authors contributed equally to this work.

<https://doi.org/10.1016/j.redox.2021.101971>

Received 18 January 2021; Received in revised form 22 March 2021; Accepted 8 April 2021

Available online 17 April 2021

2213-2317/© 2021 The Author(s).

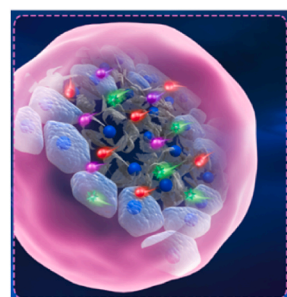
Published by Elsevier B.V. This is an open access article under the CC BY-NC-ND license

(<http://creativecommons.org/licenses/by-nc-nd/4.0/>).

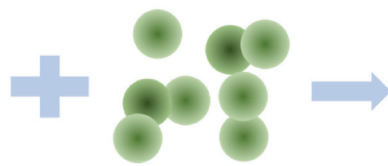
peroxidation contingent on reactive oxygen species (ROS) levels and the availability of iron [12]. Recently, RPE ferroptosis induced by GSH depletion, tBH incubation, or direct ferrous iron supplementation was demonstrated as a major pattern of oxidative stress-mediated RPE cell death [13–15]. Nevertheless, the fundamental mechanisms underlying the pathogenic processes and the cumulative effects of oxidative stress-mediated RPE ferroptosis and subsequent photoreceptor damage are not well elucidated.

Considering AMD therapeutics, the limitations of available anti-vascular endothelial growth factor treatments for neovascular (wet) AMD and the nearly complete lack of effective options for non-neovascular (dry) AMD drive a continuing demand for improved therapeutics [16]. Heme oxygenases (HO), as an inducible enzyme, is considered a measurable indicator of oxidative stress, which oxidize cellular heme to carbon monoxide (CO), biliverdin, and free ferrous iron [17]. The HO reaction may either exhibit cytoprotection by converting prooxidant hemoproteins and heme to the antioxidant biliverdin and biliverdin or, conversely, exacerbate oxidative stress by releasing ferrous iron and CO [17]. Thus, the two-sided effect implicates HO-1 as a double-edged sword in to afford protection or enhance vulnerability in various experimental models [18,19]. It has been reported that induction of HO-1 has positive effects on retinal degeneration [20]. For instance, HO-1 induction exerts a protective effect in retinal endothelial cells after exposure of hyperglycemic and oxidative/nitrosative stress conditions [21]. Recently, several reports have revealed that Nrf2/HO-1 role in ferroptosis is controversial by its anti-ferroptotic/protective or pro-ferroptotic role in various *in vitro* models such as epithelial cells, and *in vivo* models [22–26]. Thus, it is necessary to further elucidate the exact role (protection or detriment) of HO-1 induction in NaIO₃-mediated RPE oxidative stress model (mimicking many features of AMD) [27], which may provide potential therapeutic strategy to control AMD.

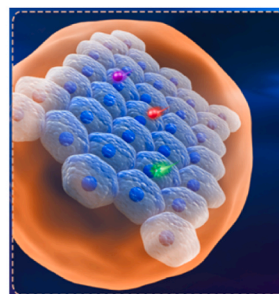
The pathogenesis ambiguity underlying oxidative stress-mediated RPE degeneration and therapeutic challenges call for a more in-depth exploration of the underlying mechanisms. In this study, by sophisticated high-throughput sequencing and biochemical evaluations, we have elaborately resolved the dominant ferroptosis-related genetic pathway in NaIO₃-mediated RPE oxidative stress model. Based on the ferroptotic RPE with HO-1 overexpression and labile ferrous perturbation, the knockdown of HO-1 or using HO-1 inhibitor ZnPP has shown to significantly rescue ferroptotic RPE dysfunction and subsequently prevent photoreceptor degeneration (Scheme 1). Our findings not only provide a novel perspective on RPE pathogenesis, but also propose an effectively targeted treatment strategy by inhibiting HO-1-mediated ferroptosis that will be clinically promising to prevent RPE dysfunction and subsequent photoreceptor degeneration in early-stage AMD patients.



Ferroptotic RPE



HO-1 inhibitor (ZnPP)



ZnPP-treated RPE

degeneration.

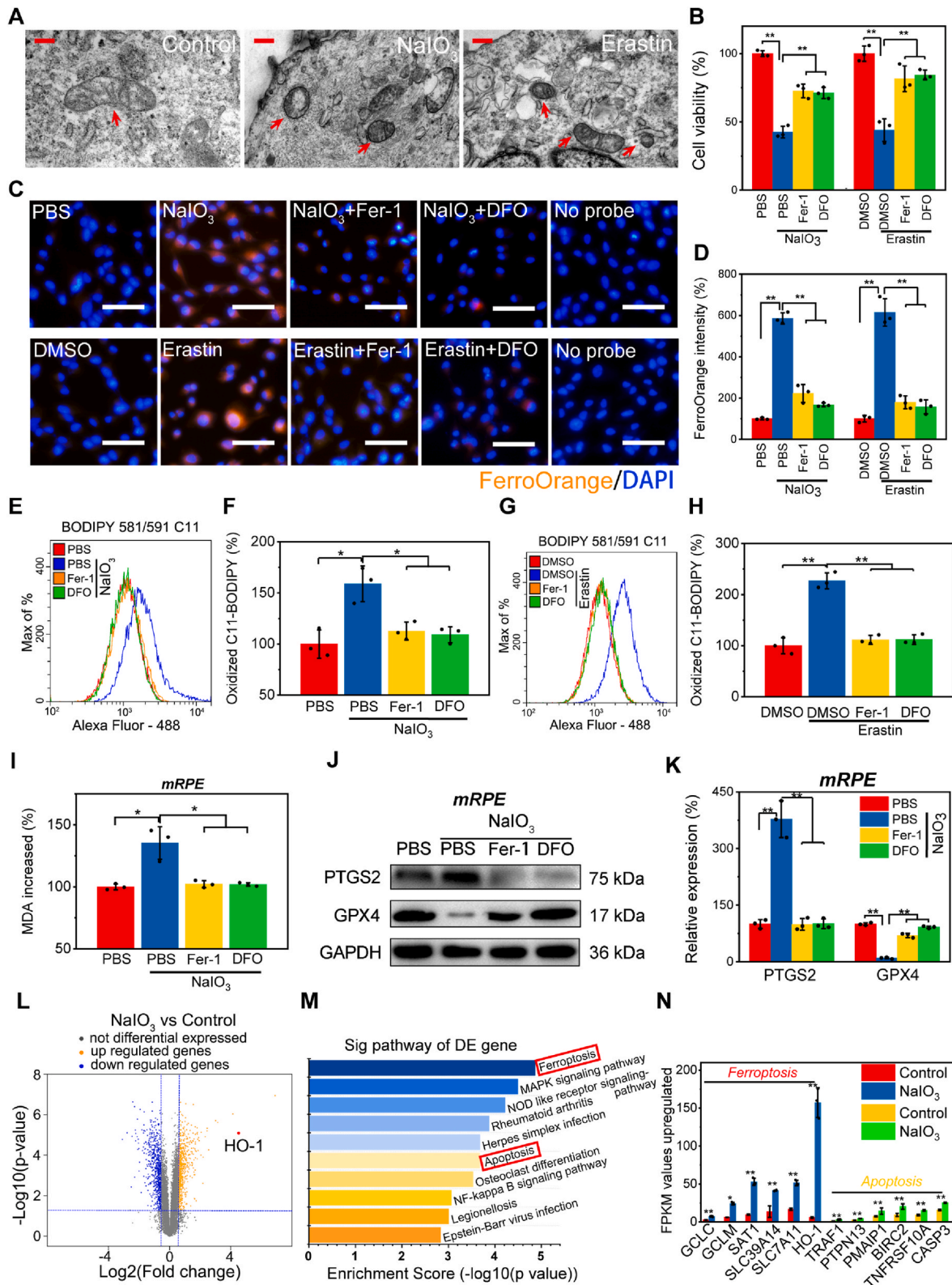
2. Results and discussion

2.1. Ferroptosis is a major pathological process in oxidative stress-mediated RPE degeneration

To appropriately determine RPE cell fates and provide insight into the underlying mechanisms of RPE under oxidative stress, NaIO₃ has been used to selectively induce RPE abnormality for establishment of oxidative stress-RPE model, which mimic many features of AMD, including the secondary cardinal phenotypes of photoreceptor degeneration [28]. We examined whether NaIO₃-induced cell death shared morphological, biochemical, or other similarities with Erastin-mediated ferroptosis (served as the positive control). By transmission electron microscopy (TEM), we observed that human retinal pigment epithelium (ARPE-19) cells treated with NaIO₃ or Erastin for 24 h exhibited the distinctive morphological features of smaller mitochondria with increased membrane density (mitochondria marked by red arrows) (Fig. 1A), consistently with a previous report [29]. To investigate the rescue effects of ferroptosis inhibitor (ferrostatin-1 (Fer-1) and deferoxamine (DFO)), the cell viability by CCK-8 analysis was determined in NaIO₃- or Erastin-treated ARPE-19 cells. Significant rescue effects on NaIO₃- and Erastin-induced cell death were observed by treating cells with Fer-1 or DFO. These results suggested that NaIO₃ treatment induced a high proportion of ferroptotic cell death (Fig. 1B). The catalytic role of iron in ferroptosis has been highlighted [30,31]. By staining cells with FerroOrange (to detect ferrous ions), we found that NaIO₃ and Erastin-treated cells accumulated excessive ferrous ions, which were significantly blocked by pre-incubation with Fer-1 or DFO, as revealed by the decreased orange fluorescence (Fig. 1C and D). Cellular iron accumulation is one of the typical hallmarks of ferroptosis, as ferrous ion accumulation could specifically increase detrimental oxidative stress levels, including ROS and lipid ROS (LOS) [32]. Subsequently, the increased LOS levels in NaIO₃- (Fig. 1E and F) and Erastin-treated cells (Fig. 1G and H) were assayed by flow cytometry using the fluorescent probe C11-BODIPY. Substantial attenuation of LOS accumulation was observed when cells were co-incubated with Fer-1 or DFO. Consistently with recent reports on ferroptosis induction [13,14]. NaIO₃-induced RPE cell death was also accompanied by ferroptosis-associated characteristics, such as ferrous iron accumulation and lipid peroxidation, which could be significantly attenuated by DFO and Fer-1. Together with the shrunken mitochondria observed in RPE cells after NaIO₃ treatment, these results indicate that ferroptosis is a major pathological process involved in NaIO₃ oxidative stress-mediated RPE cell death.

To further investigate the oxidative stress-mediated RPE cell fate, *in vivo* monolayer mouse RPE (mRPE) cells from NaIO₃-treated retinac were evaluated. With respect to the levels of malondialdehyde (MDA), the most prevalent byproduct of LOS [33], we found that the mRPE in mice treated with NaIO₃ exhibited significantly elevated LOS levels, as

Scheme 1. HO-1-mediated ferroptosis as a target for protection against retinal pigment epithelium degeneration. Left panel: RPE ferroptosis is a major pathological process responsible for NaIO₃-induced retinal oxidative stress, which is mainly mediated by a vicious cycle between HO-1 upregulation and iron overload with lethal oxidative stresses of ROS/LOS accumulation. Green ball: ferrous ions; red ball: ROS; purple ball: LOS. Right panel: HO-1 inhibitor ZnPP inhibits RPE ferroptosis by specifically inhibiting HO-1 overexpression, and hampering the detrimental circulative effects between HO-1 and ferrous ion to decrease LOS and ROS overload, eventually suppressing RPE death and subsequent photoreceptor



(caption on next page)

Fig. 1. Ferroptosis is a major pathological process in oxidative stress-mediated RPE degeneration. (A) Ultrastructure of mitochondria in ARPE-19 cells treated with Erastin (5 μ M) and NaIO₃ (30 mM) for 24 h was imaged by TEM. Red arrowheads: shrunken mitochondria. Scale bars, 0.5 μ m. ARPE-19 cells were pretreated with ferroptosis inhibitors (Fer-1, 10 μ M and DFO, 75 μ M) for 1 h followed by NaIO₃ and Erastin treatment, 24 h later, (B) cell viability detected by CCK-8, (C) ferrous ion levels by FerroOrange staining and (D) corresponding quantification by Image J were evaluated. Scale bars, 50 μ m n = 3, means \pm SD; one-way ANOVA with Bonferroni correction; **P < 0.01. Flow cytometry plots and bar graphs of lipid ROS (LOS) production in (E, F) NaIO₃- and (G, H) Erastin-treated ARPE-19 cells using C11-BODIPY were showed. n = 3, means \pm SD; one-way ANOVA with Bonferroni correction; *P < 0.05, **P < 0.01. *In vivo* mRPE cells were pretreated with Fer-1 or DFO followed by NaIO₃ and Erastin treatment, 2 weeks later, (I) MDA analysis for evaluation of LOS levels, (J) protein blots and (K) semi-quantitation of the protein expression levels of ferroptosis biomarkers PTGS2 and GPX4 were determined. n = 3, means \pm SD; one-way ANOVA with Bonferroni correction; *P < 0.05, **P < 0.01. (L–N) RNA-sequencing analysis of PBS (control) and NaIO₃-treated ARPE-19 cells for 24 h. (L) The number of genes in differential expressions (\geq 1.5-fold difference: upregulated (yellow) and downregulated genes (blue)) was presented in volcano plot. (M) KEGG enrichment analysis identified the most significantly affected pathways in response to NaIO₃ treatment in differentially expressed genes. (N) FPKM values of main regulators in ferroptosis and apoptosis after NaIO₃ incubation. n = 3, mean \pm SD; two-tailed *t*-test; *p < 0.05 and **p < 0.01. (For interpretation of the references to color in this figure legend, the reader is referred to the Web version of this article.)

revealed by high colorimetric values, and pretreatment with Fer-1 and DFO significantly suppressed the LOS accumulation (Fig. 1I). To further verify NaIO₃-induced ferroptosis in mRPE, we measured the levels of the ferroptosis markers, glutathione peroxidase 4 (GPX4) and prostaglandin-endoperoxide synthase 2 (PTGS2) [34]. Relative to untreated retinae, NaIO₃-treated mRPE showed about 4-fold increases PTGS2 protein expression levels, and caused a downregulation of GPX4 protein levels (Fig. 1J and K). Consistently with the results *in vitro*, these phenomena could be reversed by Fer-1 and DFO treatment, further emphasizing that ferroptosis plays an essential role in oxidative stress-mediated RPE cell death.

Furthermore, RNA-sequencing technique was performed to determine the RPE cell death types induced by NaIO₃. After ARPE-19 cells treatment with NaIO₃, 637 genes were significantly downregulated and 661 genes were significantly upregulated compared with the control cells as illustrated in volcano plot and heatmap (Figure 1L, S1). Kyoto encyclopedia of genes and genomes (KEGG) enrichment analyses of the differentially expressed genes showed that ferroptosis ranked as the top pathway, *i.e.*, higher than apoptosis, upon NaIO₃ treatment, and necroptosis-related genes were not enriched (Figure 1M). These results were validated by the higher gene level fragments per kilobase of exon per million fragments (FPKM) values of the main ferroptosis regulators compared with apoptotic factors (Figure 1N). The above evidence strengthens the idea that ferroptosis is a major pathological process involved in oxidative stress-induced RPE cell death. Therefore, in-depth studies of the ferroptotic pathogenesis relevant to RPE and the rationally targeted therapeutic strategy for clinical practice are urgently needed.

2.2. Excessive activation of HO-1 via Nrf2–SLC7A11–HO-1 hierarchy contributes to RPE ferroptosis

The differentially expressed genes that are closely associated with RPE ferroptosis were analyzed by RNA-sequencing (Fig. S1). Among them, heme oxygenase-1 (*HMOX1*, also known as *HO-1*) and solute carrier family 7 member 11 (*SLC7A11*) were identified as the most dramatically upregulated genes in NaIO₃-treated RPE cells (Fig. 2A), as further validated by qPCR, western blot, and immunocytochemistry (ICC) analysis (Fig. 2B and C and S2, S3A, B). The gene ontology (GO) molecular function analysis also revealed that NaIO₃ mainly affected the expression of HO-1, which plays a predominant role in cellular signaling and the regulation of the response to stress (Fig. S4). It has been documented that HO-1 expression is controlled by several transcription factors, including nuclear factor erythroid 2-related factor 2 (Nrf2), Yin Yang 1 (YY1), activator protein-1 (AP-1), hypoxia-inducible factor-1 α (HIF-1 α), and signal transducer and activator of transcription 3 (STAT3) [22]. Among these transcription factors, significant upregulation of only Nrf2 was observed, implying that the upregulation of HO-1 expression is predominantly coordinated by Nrf2 in NaIO₃-treated cells (Fig. 2D and E). Significantly increased Nrf2 mRNA expression level and Nrf2-stained positive cells were also observed in ARPE-19 cells after NaIO₃ exposure (Figs. S5, S6A, B). It has been reported that, upon nuclear translocation, Nrf2 can interact with SLC7A11 to activate transcription of the target

gene HO-1 in ferroptotic cancer cells [35]. To further understand the molecular events that may result in the abnormality documented above, we isolated mRPE monolayer cells from NaIO₃-treated mice and analyzed the total mRNA and protein expression profiles of Nrf2, SLC7A11, and HO-1. We observed increased expression of SLC7A11, at both mRNA and protein levels, in line with the upregulation of Nrf2 and HO-1 in NaIO₃-treated retinae (as observed by qPCR and immunofluorescence [IF] assays) (Fig. 2F, G and S7), indicating that the Nrf2–SLC7A11–HO-1 pathway is activated in NaIO₃-induced ferroptotic RPE cells. To further validate the relationship between Nrf2, SLC7A11, and HO-1 in RPE ferroptosis, functional RNAi knockdown studies with siNrf2, siSLC7A11, and siHO-1 were conducted (Figs. S8A–F). As shown in Fig. 2H and I, Nrf2 knockdown blunted the increases in SLC7A11 and HO-1 levels in NaIO₃-treated ARPE-19 cells, whereas SLC7A11 knockdown only attenuated the upregulation of HO-1, without significantly affecting Nrf2 levels (Fig. 2J and K). In addition, HO-1 knockdown showed no significant effects on both Nrf2 and SLC7A11 levels (Figure 2L, M), emphasizing the regulatory hierarchy of Nrf2–SLC7A11–HO-1 in NaIO₃-induced RPE ferroptosis.

SLC7A11, as an important role in the ferroptotic process [29], is a cystine/glutamate antiporter, and the cystine imports is essential for the synthesis of glutathione (GSH) [29]. Previous studies reported that some ferroptosis inducers (*e.g.*, Erastin) could deplete GSH levels by serving as a SLC7A11 inhibitor and cause the compensatory increase in SLC7A11 levels [36]. However, in contrast to Erastin treatment, we did not find a significant decrease in GSH levels in NaIO₃-induced RPE cells (Fig. S9A), in agreement with previous results in tumor cells caused by ferroptosis inducers (*e.g.*, RSL3 and withaferin A) [37,38], indicating that the activation of SLC7A11 induced by NaIO₃ may not be a compensatory upregulation to increase GSH levels. In this study, increased levels of SLC7A11 and HO-1 were observed after NaIO₃ induction. To explore the relationship between SLC7A11 and HO-1, siRNA was utilized to knock down SLC7A11 and lentiviruses were used to overexpress SLC7A11 (Fig. S9B). Western blot results showed that SLC7A11 knockdown significantly blunted the NaIO₃-induced increase in HO-1 levels (Fig. 2J and K). Conversely, SLC7A11 overexpression enhanced the upregulation of HO-1 expression levels in NaIO₃-treated RPE cells (Fig. S9C), suggesting that SLC7A11 positively regulates HO-1 expression after NaIO₃ treatment. As reported, induction of the Nrf2 pathway, especially with SLC7A11 and HO-1 activation through oxidative agents, may contribute to the iron-dependent and oxidative stress-induced cell death [35]. Herein, NaIO₃ significantly elevated HO-1 expression and did not significantly change the GSH levels, in contrast to Erastin, which significantly reduced GSH levels and failed to increase HO-1 expression (Figs. S9A and D), suggesting that Erastin and NaIO₃ treatment initiate RPE ferroptosis in different ways. Collectively, the upregulation of HO-1 is coordinated by the Nrf2–SLC7A11–HO-1 hierarchy in oxidative stress-mediated RPE ferroptosis.

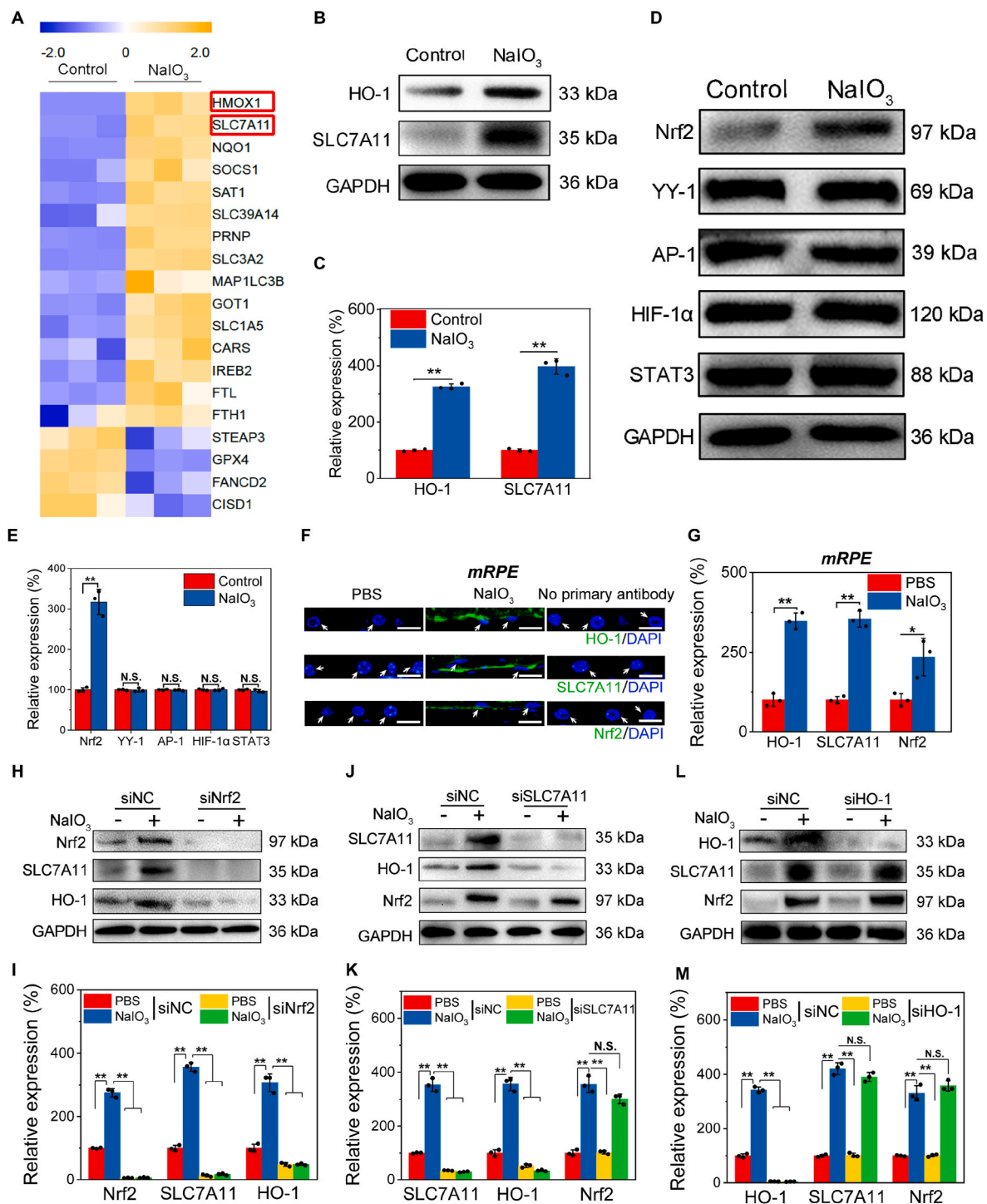


Fig. 2. Excessive activation of HO-1 via Nrf2–SLC7A11–HO-1 hierarchy contributes to RPE ferroptosis. (A) Differentially expressed genes that are closely associated with RPE ferroptosis in NaIO₃-treated cells were determined by RNA-sequencing analysis. Blue: low expression levels. Yellow: high expression levels. (B) Protein blots and (C) semi-quantitation of the protein expression levels of HO-1 and SLC7A11 in ARPE-19 in response to NaIO₃ were examined. $n = 3$, means \pm SD; two-tailed t -test; ** $P < 0.01$. (D) Protein expression levels and (E) semi-quantitation of HO-1 upstream, including Nrf2, YY1, AP-1, HIF-1 α , and STAT3 were analyzed by western blot. $n = 3$, means \pm SD; two-tailed t -test; ** $P < 0.01$, N.S., not significant. (F) IF staining and (G) corresponding quantification of the relative expression of Nrf2, SLC7A11 and HO-1 were performed in mRPE after NaIO₃ treatment for 2 weeks. Scale bars, 20 μ m, $n = 3$, means \pm SD; two-tailed t -test; * $P < 0.05$, ** $P < 0.01$. By western blot and further semi-quantitation analysis, relationship of Nrf2, SLC7A11 and HO-1 in RPE ferroptosis was identified by knockdown of (H, I) Nrf2 (siNrf2), (J, K) SLC7A11 (siSLC7A11), and (L, M) HO-1 (siHO-1) in ARPE-19 cells followed by NaIO₃ treatment. $n = 3$, means \pm SD; one-way ANOVA with Bonferroni correction; ** $P < 0.01$, N.S., not significant. (For interpretation of the references to color in this figure legend, the reader is referred to the Web version of this article.)

2.3. HO-1 upregulation elicits cellular ferrous accumulation to boost RPE ferroptosis

The apparent discrepancy between protective anti-oxidant effects [20,21] and detrimental pro-oxidant [39–41] of HO-1 in various tissues and pathologic processes has been underscored. Functional analyses of HO-1 induction by transfection of HMOX1 cDNA (hHO-1) have been performed to further characterize the role of HO-1 during ferroptotic pathogenesis of RPE cells (Figs. S10A and B). As presented in Fig. 3A–D, and S11, direct transfection with hHO-1, similar to NaIO₃ induction in ARPE-19 cells, led to a higher cell mortality, an intense ferrous fluorescence intensity, and an approximately 4-fold increase in LOS levels compared with control cells, which could be strongly reversed in cells pretreated with the HO-1 inhibitor zinc protoporphyrin-9 (ZnPP). Based on the established 3D tri-layer model (primary human umbilical

vein-derived endothelial cells (HUVEC) + ARPE-19 co-culture) (Figs. S12A and B), the effect of HO-1 overexpression on RPE cell permeability was further analyzed by measuring the leakage (diffusion rate) of fluorescein isothiocyanate (FITC)-dextran. It has been found that HO-1 overexpression in ARPE-19 cells induced a significantly increased diffusion rate compared to normal 3D tri-layer model, suggesting the impaired integrity of RPE barrier after HO-1 overexpression, which could be significantly inhibited after treatment with the ZnPP (Fig. S12C). Moreover, the phagocytosis function of RPE cell is another unique function in retina to support the growth of photoreceptors. Weak fluorescence of pH-sensitive red fluorescence-conjugated *E. coli* bio-particles was observed in HO-1 overexpressed ARPE-19 cells, indicating the attenuated phagocytotic activity after HO-1 overexpression, which could be significantly promoted after incubation with ZnPP (Figs. S12D and E). HO-1 detoxifies heme into biliverdin, releasing ferrous ions and

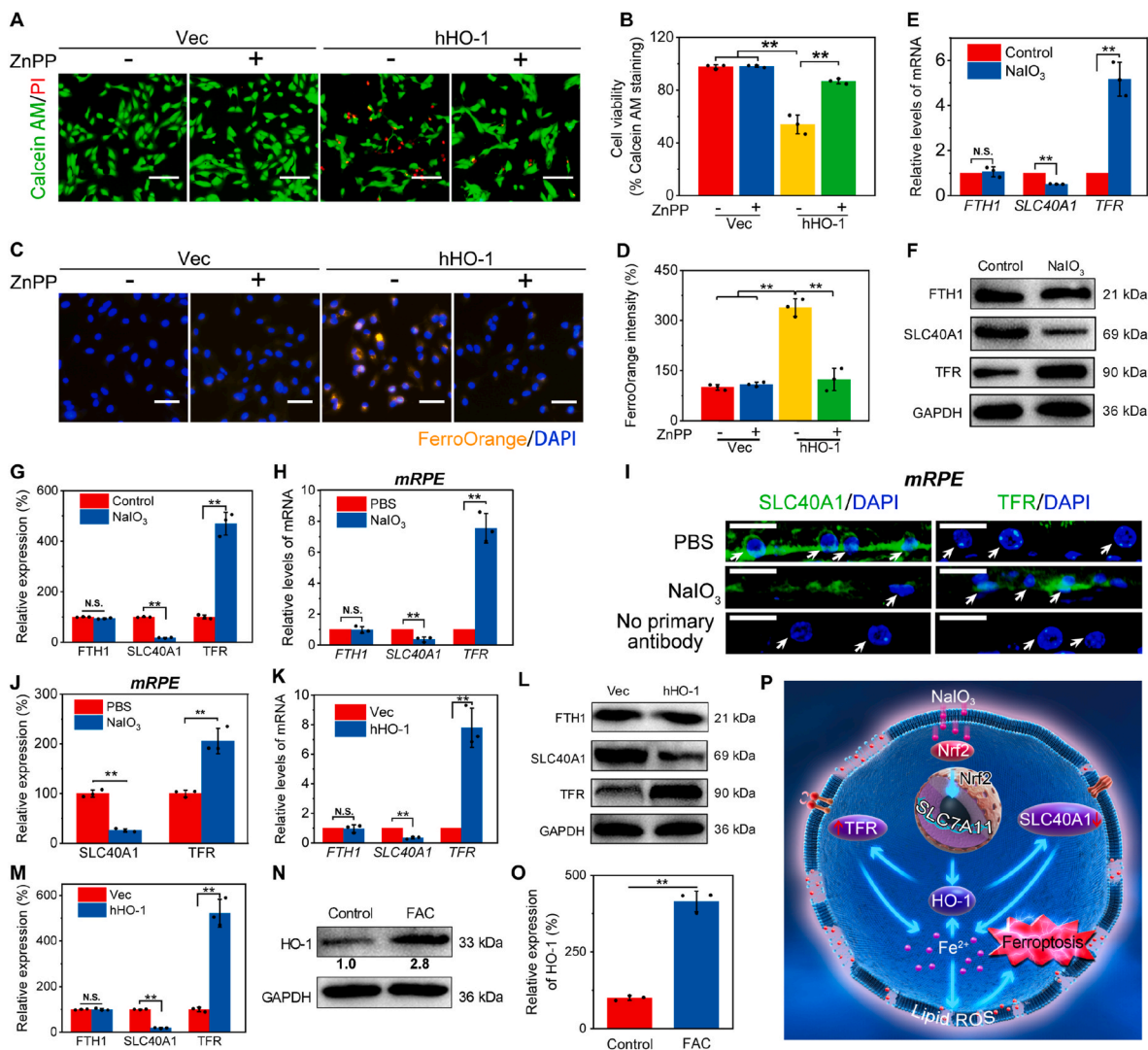


Fig. 3. HO-1 upregulation elicits cellular ferrous accumulation to boost RPE ferroptosis. ARPE-19 cells were pretreated with HO-1 inhibitor zinc protoporphyrin-9 (ZnPP, 10 μ M) for 1 h followed by transfection of the hHO-1-expressed plasmid. After 24 h, (A) cell survival/death by live/dead staining (Calcein AM: live cells, PI: dead cells), (B) corresponding quantification of cell viability by Image J, (C) ferrous ion levels by FerroOrange staining and (D) corresponding quantification were determined. Scale bars, 100 μ m n = 3, mean \pm SD, one-way ANOVA with Bonferroni correction; ** p < 0.01. (E) The mRNA expression levels by qPCR, (F) protein expression levels by western blot analysis and (G) semi-quantification of iron homeostasis-related makers, FTH1, SLC40A1 and TFR in NaIO₃-treated ARPE-19 cells were performed. n = 3, mean \pm SD, two-tailed t -test, ** p < 0.01, N.S., not significant. (H) The mRNA expression levels of FTH1, SLC40A1 and TFR by qPCR, (I) protein expression levels by IF analysis and (J) relative quantification of SLC40A1 and TFR were evaluated in mRPE from NaIO₃-treated retiniae. Scale bars, 20 μ m n = 3, mean \pm SD, two-tailed t -test, ** p < 0.01, N.S., not significant. (K) The mRNA expression levels by qPCR, (L) protein expression levels by western blot analysis and (M) semi-quantification of FTH1, SLC40A1 and TFR in ARPE-19 cells transfected with the hHO-1-expressed plasmid were performed. n = 3, mean \pm SD, two-tailed t -test, ** p < 0.01, N.S., not significant. (N) Western blot analysis and (O) semi-quantification of HO-1 in protein levels were evaluated in ARPE-19 after FAC incubation (250 μ mol/L) for 24 h. (P) Scheme of detailed mechanism in NaIO₃-induced RPE ferroptosis.

carbon monoxide [17]. To further understand the role of hemin in regulating HO-1, we treated the ARPE-19 cells with hemin at different concentration (2, 5 and 10 μM) and analyzed the HO-1 expression, ferrous ion level and cell viability. We found a concentration-dependent increase of HO-1 in protein level in response to hemin (Figs. S13A and B), whereas 10 μM , but not 2 and 5 μM hemin significantly reduced the cell viability and elevated the ferrous ion level (Figs. S13C–E), suggesting that the extracellular hemin exerts cytotoxic effect in ARPE-19 cells due to the significantly upregulated HO-1 expression but not the slight increase of HO-1 induced by hemin. Additionally, administration of hemin in NaIO_3 -treated ARPE 19 cells induced a stronger upregulation of HO-1 than NaIO_3 alone (Figs. S13F and G), further sensitized NaIO_3 -induced cell death and aggravated ferrous ion overload (Figs. S13H–J). The results revealed that the high intensity of HO-1 induction by hemin determines the free radical damage resulting from the intracellular release of iron, which is consistent with that hemin/HO-1

sensitizes withaferin A-induced ferroptotic cell death in cancer cells [42].

Intracellular iron homeostasis is balanced through ferroportin (encoded by solute carrier family 40 member 1, *SLC40A1*) for iron export, transferrin receptor (encoded by transferrin receptor, *TFR*) for iron import, and ferritin (encoded by, e.g., ferritin heavy chain 1, *FTH1*) for iron storage [35,43]. As shown in Fig. 3E–G, NaIO_3 -treated ARPE-19 cells showed significant upregulation of TFR and downregulation of *SLC40A1* at the mRNA and protein levels, without significantly affecting the *FTH1* levels, which is in line with the observed trend in mRPE from NaIO_3 -induced retinae (Fig. 3H–J). Similarly, it has been evidenced that hHO-1-transfected-ARPE-19 cells significantly upregulated TFR and downregulated *SLC40A1* at the mRNA and protein levels, and nearly unchanged the *FTH1* levels (Fig. 3K–M). These outcomes suggest that iron accumulation is mainly regulated by the altered expression levels of TFR and *SLC40A1*, which is attributed to the upregulation of HO-1. The

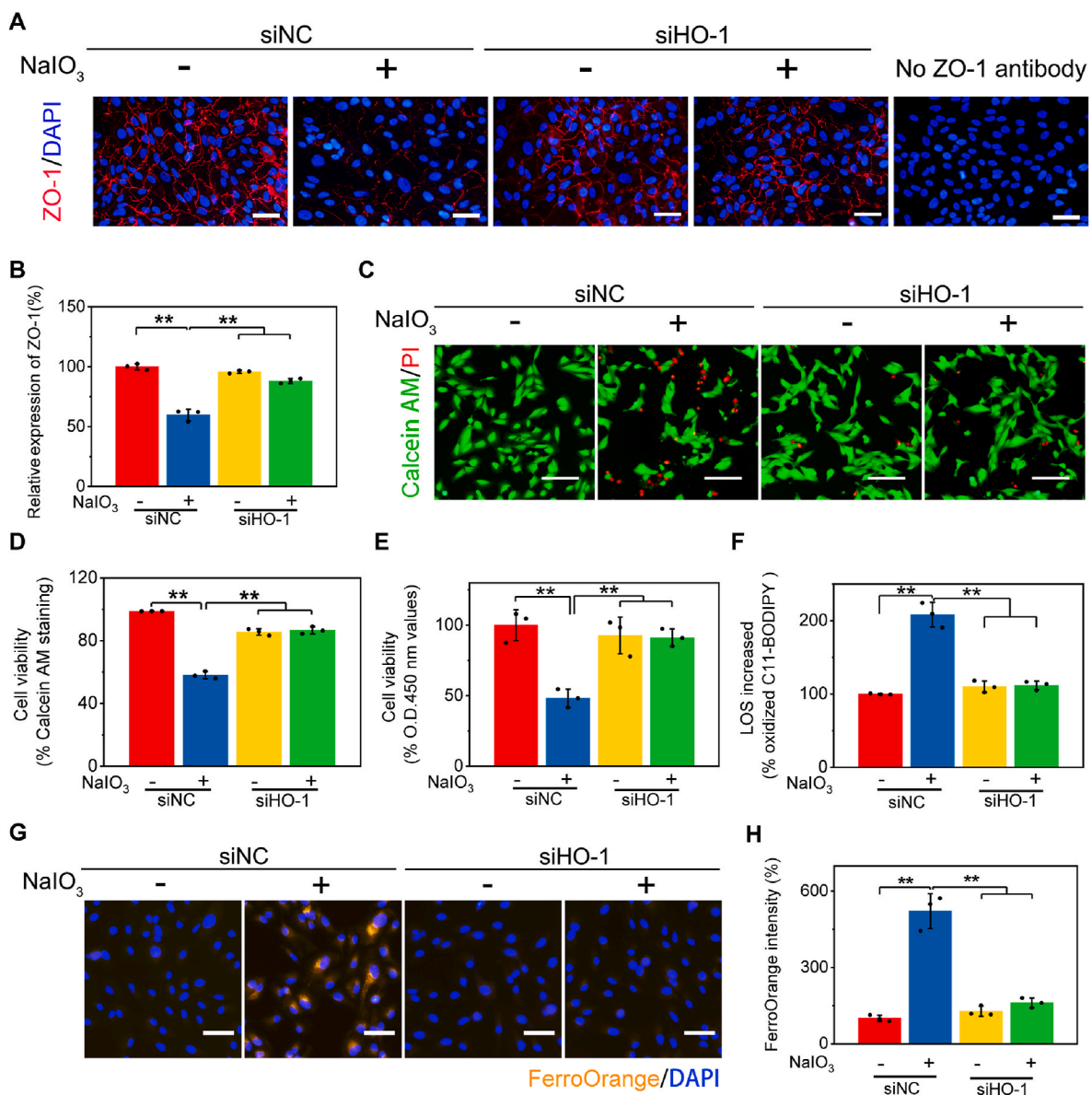


Fig. 4. Inhibiting HO-1 overexpression protects against RPE ferroptosis *in vitro*. HO-1 knockdown ARPE-19 cells were treated with NaIO_3 for 24 h, followed by evaluation of (A) protein expression of ZO-1 by ICC staining and (B) relative quantification, (C) cell survival/death by live/dead staining (Calcein AM: live cells, PI: dead cells), (D) corresponding cell viability quantification, and (E) further quantification of cell viability by CCK-8 analysis. Scale bars, 50 μm in (A), 100 μm in (C). $n = 3$, mean \pm SD, one-way ANOVA with Bonferroni correction; $**p < 0.01$. (F) Intracellular LOS levels by C11-BODIPY staining, (G) ferrous staining by FerroOrange probe and (H) corresponding quantification were carried out in siHO-1-infected ARPE-19 cells with NaIO_3 treatment for 24 h. Scale bars, 100 μm $n = 3$, means \pm SD; one-way ANOVA with Bonferroni correction; $**p < 0.01$.

excessive activation of HO-1 specifically exerted a pro-oxidative effect in RPE ferroptosis and is responsible for the massive ferrous ion accumulation. To further explore the potential relationship between HO-1 and ferrous iron, direct ferrous iron supplementation using ferric ammonium citrate (FAC) was performed. Directly, we found that FAC significantly induced ferrous iron overload and increased *PTGS2* mRNA expression in ARPE-19 cells (Figs. S14A–C). Interestingly, the excessive labile iron levels after treatment with FAC could in turn dramatically enhance HO-1 protein expression in ferroptotic RPE cells, as revealed by western blot and ICC analyses (Figure 3N, O, and S15A, B). Collectively, our data demonstrate that upregulation of HO-1 by the Nrf2–SLC7A11–HO-1 pathway stimulates TFR upregulation and SLC40A1 downregulation, eliciting intracellular ferrous accumulation and boosting iron-dependent RPE ferroptosis. In turn, labile iron accumulation augments HO-1 expression, propagating a vicious cycle between HO-1 upregulation and iron accumulation, exacerbating RPE ferroptosis (Figure 3P), which provide important clues to block RPE ferroptosis by inhibiting HO-1 overexpression or decreasing accumulative iron levels.

2.4. Inhibiting HO-1 overexpression protects against RPE ferroptosis *in vitro*

To illustrate whether inhibiting HO-1 overexpression exhibits the therapeutic performance against RPE ferroptosis, functional analyses of HO-1 using knockdown (siHO-1) have been performed. Immunofluorescence results showed that the protein expression levels of ZO-1 (RPE cell tight junction biomarker) in NaIO₃-induced ARPE-19 cells were distinctively lower, and siHO-1-transfected cells followed by NaIO₃ treatment showed no significant difference in ZO-1-stained positive cells compared with the control vector group (siNC), as evidenced by the not significantly diminished ZO-1 abundance at many cell boundaries (Fig. 4A and B). Additionally, the abnormal morphology and repressed cell viability after NaIO₃ treatment were not obviously detected in siHO-1-transfected ARPE-19 cells (Fig. 4C–E). As indicated, NaIO₃ treatment obviously decreased the cell viability by about 50% in RPE cells, while did not affect the cell viability in siHO-1-transfected RPE cells by live/dead staining (Fig. 4C and D), which was also validated by a CCK-8 analysis (Fig. 4E). In addition, siNC-transfected cells followed by NaIO₃ treatment for 24 h resulted in a significantly increased FITC-dextran diffusion rate and compromised RPE phagocytosis, which could be obviously reversed by HO-1 inhibition using siHO-1 transfection (Figs. S16A–C). These data preliminarily implying that inhibiting HO-1 overexpression is beneficial for protecting against RPE cell ferroptosis *in vitro*. To specifically analyze the alteration of ferroptosis-associated biomarkers by inhibiting HO-1 overexpression, the effects of siHO-1 transfection on cellular total LOS and ferrous ion levels in ARPE-19 cells followed by NaIO₃ treatment were also investigated. Compared to the vector group, no significant increase of LOS was detected in the siHO-1 transfection group followed by NaIO₃ exposure (Fig. 4F), indicating that siHO-1 transfection was also proved to be sufficient to inhibit the burst in oxidative stress in NaIO₃-treated ARPE-19 cells. Furthermore, cellular ferrous ion evaluation results showed that the fluorescence intensity of FerroOrange-stained-cells were much higher in NaIO₃ group without HO-1 knockdown, in contrast to that transfection with siHO-1, suggesting that inhibiting HO-1 overexpression dramatically ameliorated NaIO₃-induced iron accumulation and possessed the strong iron-reducing capability by HO-1 knockdown (Fig. 4G and H). These findings implicate that inhibiting HO-1 overexpression by transfection with siHO-1 effectively suppresses oxidative stress-mediated RPE ferroptosis *in vitro*.

2.5. Inhibiting HO-1 overexpression protects against RPE ferroptosis and photoreceptor degeneration *in vivo*

To further examine whether inhibiting HO-1 overexpression possesses high *in vivo* therapeutic efficacy consistent with that exhibited *in*

vitro, ZnPP (50 mg/kg) was administered intraperitoneally once a week to inhibit HO-1 overexpression in NaIO₃-induced mice [44]. We found that intraperitoneal injection of ZnPP followed by NaIO₃ treatment for 2 weeks significantly decreased the HO-1 expression levels (Fig. 5A and B). The effects of ZnPP on the expression levels of biomarkers of the visual recycle in RPE cells, e.g., RPE65 and RLBP1, were detected in mRPE after NaIO₃ injection, which are associated with the photoreceptor response to light stimulation [45]. Fortunately, the reduced protein levels of RLBP1 and RPE65 in ferroptotic mRPE from NaIO₃-treated retinæ were increased with ZnPP pretreatment (Fig. 5A and B). H&E staining additionally showed the abnormal hypopigmentation and hyperpigmentation, as well as largely loss and swelling of RPE in NaIO₃-treated retinæ (mRPE marked by red arrows), which were significantly rescued after pretreatment with ZnPP (Fig. 5C), suggesting the satisfactory effects obtained upon inhibiting HO-1 overexpression. To better show the effectiveness of ZnPP in rescuing RPE cell death and morphological abnormalities, RPE flat mounts were stained for ZO-1. We observed that injection with ZnPP significantly prevented the disruption of RPE cell tight junctions in NaIO₃-treated retinæ, as evidenced by an increase in the diminished ZO-1 abundance at many cell boundaries (Fig. 5D and E). The role of HO-1 inhibition using HO-1 inhibitor ZnPP after (“ZnPP after” group) and ZnPP previous to (“ZnPP before” group) NaIO₃ administration has been further analyzed by evaluating the HO-1 expression, cell viability and ferrous ion level. Our results showed that the protein level of HO-1 in NaIO₃-treated AREP-19 cells was decreased in “ZnPP after” group, but the reduction is more significant in “ZnPP before” group (Figs. S17A and B). Compared with “ZnPP after” group, “ZnPP before” group showed greater suppression in NaIO₃-induced cell death, which is further supported by CCK-8 analysis (Figs. S17C–E). Additionally, “ZnPP before” group in NaIO₃-treated ARPE-19 cells exhibited lower ferrous ion level, as presented with weaker ferrous fluorescence than “ZnPP before” group (Figs. S17F and G). These results suggest that compared with HO-1 inhibition after NaIO₃-induced oxidative stress, HO-1 inhibition previous to NaIO₃ administration is more effective to suppress oxidative stress-mediated RPE ferroptosis. The potential mechanism may be due to that the upregulation of HO-1 elicits intracellular ferrous accumulation and boosts iron-dependent RPE ferroptosis following NaIO₃-induced oxidative stress, thus HO-1 inhibition previous to NaIO₃ administration will timely suppress oxidative stress-induced damage, and represents an efficient defensive strategy to prevent RPE degeneration [46]. On the other hand, our results showed that labile iron accumulation could in turn augment HO-1 expression, propagating a vicious cycle between HO-1 upregulation and iron accumulation, exacerbating RPE ferroptosis, thus HO-1 inhibition after NaIO₃ administration could also inhibit subsequent vicious feedback of oxidative stress and ferroptosis at some degree.

During vision-threatening advanced AMD, photoreceptors are considered to degenerate as a consequence of dysfunctional and dead RPE cells [45]. After finding that ZnPP could effectively prevent HO-1-mediated ferroptosis in RPE cells, we further evaluated the cytoprotective effects of ZnPP injection against photoreceptor degeneration from morphological and functional aspects *in vivo* after treatment with NaIO₃. At molecular level, the protein expression levels of representative photoreceptor-related markers, e.g., Rhodopsin and Arrestin, were evaluated. Western blot results showed that ZnPP elevated the protein expression levels of Rhodopsin and Arrestin compared with NaIO₃-treated retinæ (Fig. 5F and G). Consistently, immunostaining of retinal sections showed the thinning of the photoreceptor layer was associated with declined protein expression levels of Rhodopsin and Arrestin in NaIO₃-treated mice (Fig. 5H and I), indicating that the remaining photoreceptors were significantly degenerative. These phenomena could be prevented by ZnPP pretreatment, further emphasizing that inhibiting HO-1 overexpression plays an essential role in HO-1-mediated RPE ferroptosis and subsequent photoreceptor degeneration. Usually, loss of functional RPE can lead to a secondary loss of photoreceptors [45]. As

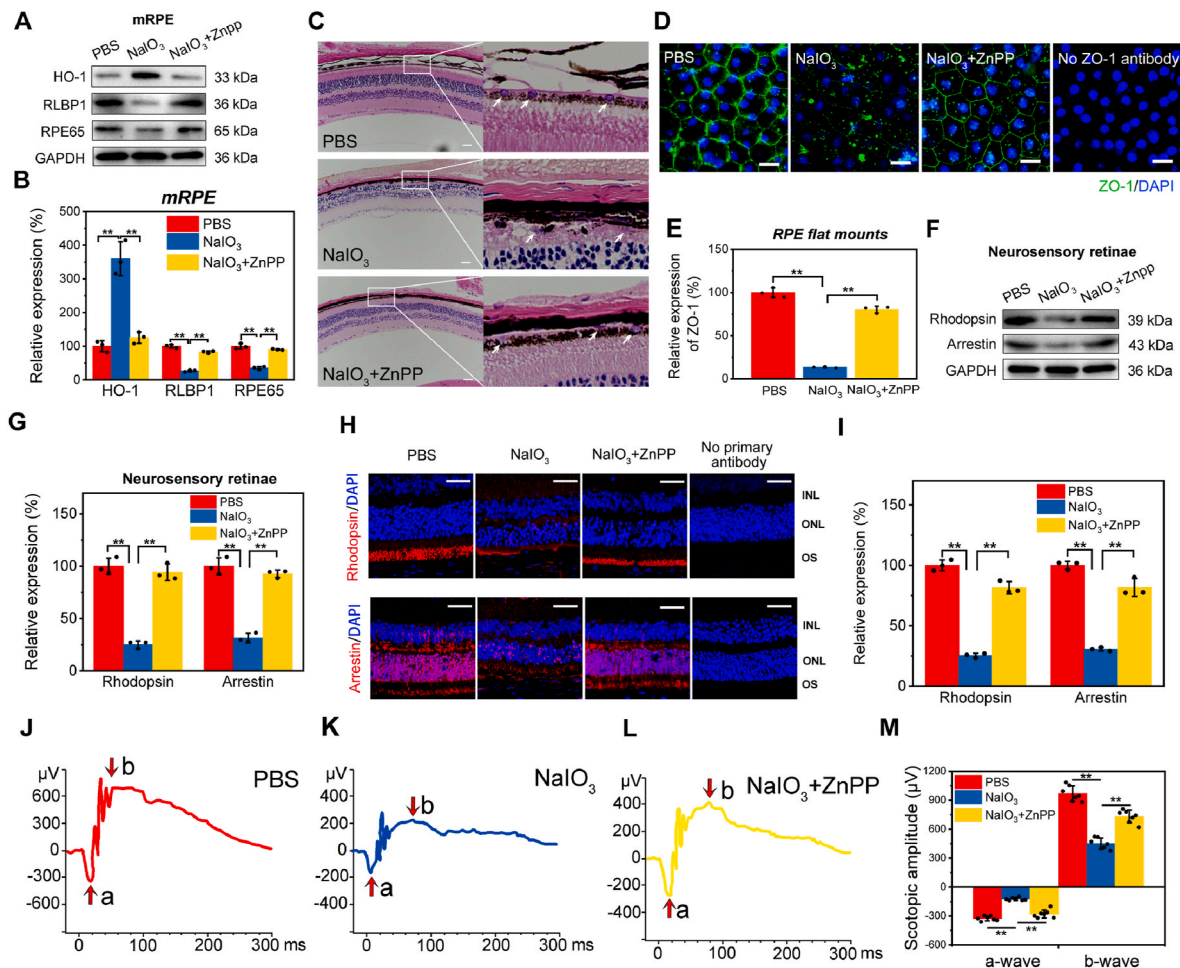


Fig. 5. Inhibiting HO-1 overexpression protects against RPE ferroptosis and photoreceptor degeneration *in vivo*. Retinae were intraperitoneally pre-treated with ZnPP (50 mg/kg) for 15 min followed by treatment with NaIO₃, 2 weeks later, (A) protein expression levels and (B) relative quantification of HO-1 and RPE visual recycle biomarkers RPE65 and RLBP1 were determined in mRPE. (C) H&E staining for RPE pigmentation and morphological changes in mRPE pretreated with ZnPP followed by NaIO₃ treatment for 2 weeks. White arrows: mRPE cells. Scale bars, 200 μ m. (D) RPE flat mounts for ZO-1 staining and (E) relative quantification were evaluated. Scale bars, 25 μ m n = 3, means \pm SD; one-way ANOVA with Bonferroni correction; **P < 0.01. Protein expression levels by (F) western blot analysis and (G) relative quantification, as well as further by (H) IF staining and (I) relative quantification of Arrestin and Rhodopsin were analyzed. OS: outer segment, ONL: outer nuclear layer, INL: inner nuclear layer. Scale bars, 50 μ m n = 3, means \pm SD; one-way ANOVA with Bonferroni correction; **P < 0.01. (J–M) Full field ERG was used to detect visual function under scotopic conditions traced from mice in (J) PBS, (K) NaIO₃, (L) NaIO₃ + ZnPP groups. (M) Scotopic-ERG a- and b-wave amplitude values by full-field ERG were measured. n = 7, mean \pm SD, one-way ANOVA with Bonferroni correction, **p < 0.01.

presented in Fig. 5H, the regions of photoreceptor in outer nuclear layer (ONL) adjacent to abnormal RPE were evidently lost in NaIO₃-treated mice, and ZnPP dramatically increased the reduced ONL thickness, further confirming the protective effects of ZnPP throughout the retinae. These outcomes especially evidence that inhibiting HO-1 overexpression is effective in repressing the progressive degeneration of retinae by morphological protection of the sophisticated retinal architecture *in vivo*.

The effect of HO-1 inhibition by ZnPP treatment on NaIO₃-induced retinal permeability was investigated by fluorescein angiography (FA) according to previous report [47]. We found that leakage of fluorescein was detected in fluorescein angiograms of NaIO₃-challenged mice at day 14, as the red arrows indicated, suggesting the disruption of RPE tight junctions and increased retinal vascular permeability. Fortunately, intraperitoneal injection of ZnPP effectively reduced NaIO₃-induced leakage, indicating a positive effect of HO-1 inhibition on protecting RPE structural integrity (Fig. S18). The ultimate goal of preservation of degenerative retinae is to protect visual function. Full-field electroretinography (ERG) was performed to test the rod photoreceptor responses to light stimulation under scotopic conditions (Fig. 5J–M). The PBS-treated mice showed a strong scotopic ERG curve as the normal

control retinal function (Fig. 5J), while NaIO₃-exposed mice exhibited a substantially reduction in ERG curve, indicating the retinal damage (Fig. 5K). Fortunately, ZnPP treatment effectively prevented NaIO₃-induced drop in a- and b-waves under scotopic conditions, reflecting an improvement in retinal function by ZnPP administration (Figure 5L). The quantification of a- and b-wave amplitudes under scotopic condition further clearly showed the retinal functional improvement followed by ZnPP treatment (Figure 5M). These data highlight that inhibiting HO-1 overexpression exerted strong protective effects on RPE cells and photoreceptors from morphological and functional aspects *in vivo*, suggesting its promising therapeutic strategy.

2.6. Inhibiting HO-1 overexpression suppresses RPE ferroptosis by decreasing cellular ferrous accumulation

To uncover the protective anti-ferroptosis mechanism of inhibiting HO-1 overexpression by ZnPP, the changed expression levels of HO-1, SLC40A1, and TFR in ferroptotic ARPE-19 cells were more rigorously investigated. The upregulated HO-1 and TFR levels and the down-regulated SLC40A1 levels were significantly reversed after ZnPP pre-treatment, at both mRNA and protein levels (Fig. 6A–C). *In vivo*,

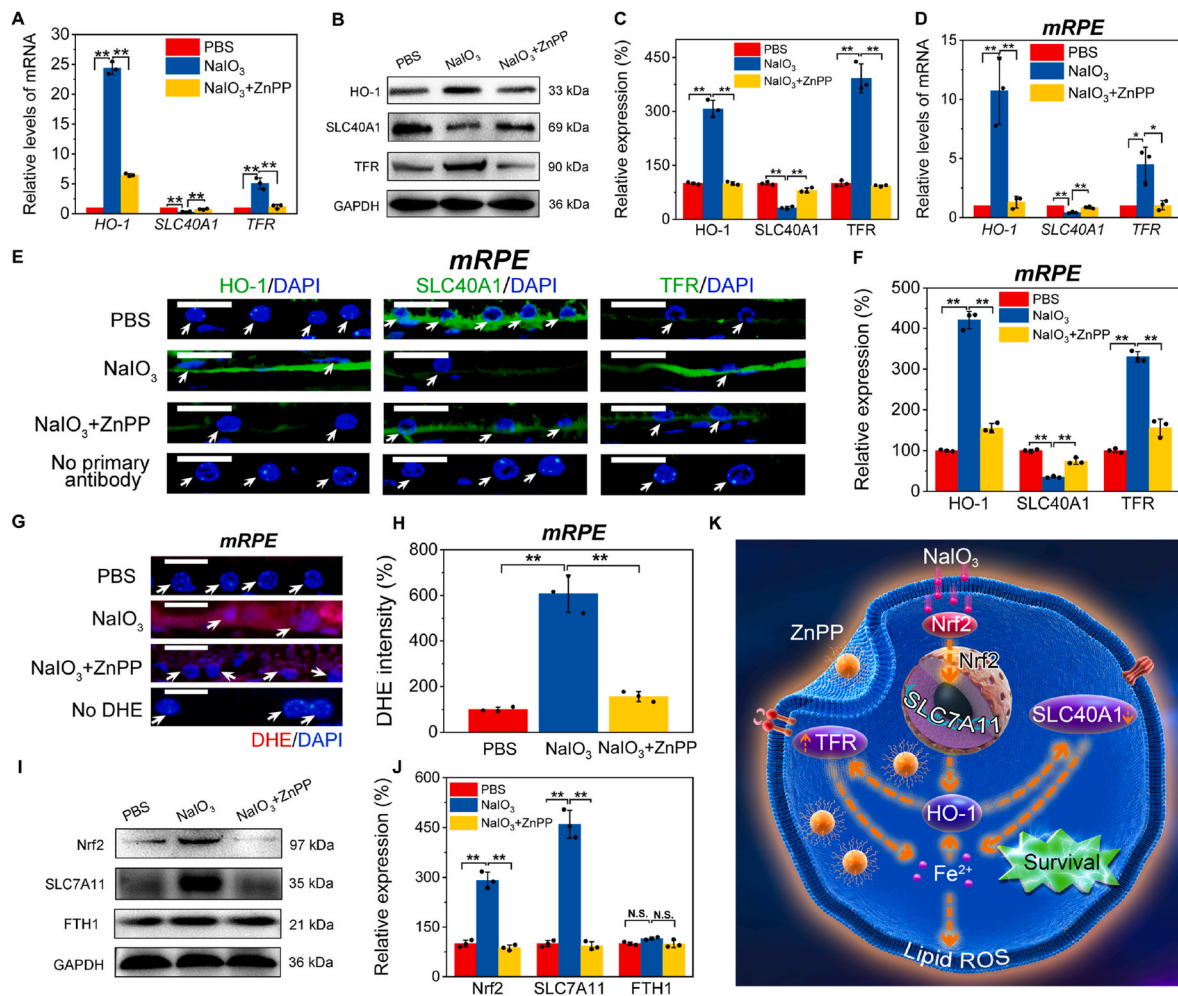


Fig. 6. Inhibiting HO-1 overexpression suppresses RPE ferroptosis by decreasing cellular ferrous accumulation. The mRPE was intraperitoneally pre-treated with ZnPP (50 mg/kg) for 15 min followed by treatment with NaIO₃, 2 weeks later, effects of ZnPP on (A) mRNA expression levels by qPCR analysis, (B) protein expression levels by western-blot analysis and (C) relative quantification of RPE ferroptosis-related markers, HO-1, SLC40A1 and TFR were evaluated in NaIO₃-treated ARPE-19 cells. $n = 3$, mean \pm SD, one-way ANOVA with Bonferroni correction, * $p < 0.05$, ** $p < 0.01$. Effects of ZnPP on (D) mRNA expression levels by qPCR analysis, (E) protein expression levels by IF staining and (F) relative quantification of HO-1, SLC40A1 and TFR were evaluated in NaIO₃-treated mRPE. Scale bars, 20 μ m $n = 3$, mean \pm SD, one-way ANOVA with Bonferroni correction, * $p < 0.05$, ** $p < 0.01$. (G) ROS levels by DHE staining and (H) quantification were evaluated in NaIO₃-treated mRPE with ZnPP treatment for 2 weeks. White arrows: mRPE monolayer cells. Scale bars, 20 μ m $n = 3$, means \pm SD; one-way ANOVA with Bonferroni correction; ** $p < 0.01$. By western blot, (I) protein blots and (J) semi-quantification of the protein expression levels of Nrf2, SLC7A11 and FTH1 were assessed in NaIO₃-treated ARPE-19 cells with or without ZnPP treatment. $n = 3$, means \pm SD; one-way ANOVA with Bonferroni correction; ** $p < 0.01$, N.S., not significant. (K) Scheme of protective mechanism of inhibiting HO-1 overexpression by ZnPP treatment against RPE ferroptosis.

intraperitoneal administration of ZnPP significantly inhibited HO-1 and TFR overexpression in mRPE from NaIO₃-treated retinas, and upregulated the SLC40A1 in mRNA and protein expression levels (Fig. 6D–F). Moreover, ZnPP also demonstrated to effectively decrease the dihydroethidium (DHE) levels (for ROS evaluation), as evidenced by decreased fluorescence intensity (Fig. 6G and H). The satisfactory effects obtained upon ZnPP treatment validate that inhibiting HO-1 overexpression could alleviate the iron-dependent RPE ferroptosis, and confirm the cytoprotective role of ZnPP by escaping the vicious feedback loop between HO-1 and ferrous ion accumulation. Importantly, the ferroptosis-related signaling proteins Nrf2 and SLC7A11, as well as iron homeostasis associated with ferroptosis, such as FTH1, were additionally assessed to further identify the anti-ferroptosis mechanism of ZnPP treatment. We found that ZnPP pretreatment could also defensively inhibit the increase of Nrf2 and SLC7A11 levels in NaIO₃-induced ARPE-19 cells (Fig. 6I and J). The phenomenon may be due to the “feedback effect” of HO-1 inhibition by ZnPP pretreatment in Nrf2-SLC7A11-HO-1 pathway, i.e., ZnPP pretreatment could inhibit HO-1 expression and subsequent vicious feedback of oxidative stress after NaIO₃

administration (Fig. 6A–H), which may further inhibit HO-1 upstream Nrf2 and SLC7A11 levels in NaIO₃-induced RPE ferroptosis. In contrast to control cells, the protein expression levels of FTH1 showed no significant change in ZnPP-treated cells, suggesting that FTH1 is unlikely to play an important role in either NaIO₃-induced ferroptosis or anti-ferroptosis mechanisms after ZnPP treatment. These data shed light on the anti-ferroptosis mechanism of inhibiting HO-1 overexpression by ZnPP treatment in NaIO₃-induced RPE cells. Overall, inhibiting HO-1 overexpression by ZnPP is capable of binding accumulative ferrous ions and further inhibiting the oxidative production, blocking RPE ferroptosis. Meanwhile, it could block the vicious circle of HO-1 upregulation and HO-1-mediated increases in iron levels by downregulating TFR and upregulating SLC40A1 in a positive feedback loop, eventually suppressing RPE ferroptosis (Fig. 6K).

3. Conclusion

In this work, we have elucidated and validated that ferroptosis, as a novel cell death form, is the major pathological process in oxidative

stress-mediated RPE death. RPE ferroptosis is induced by the upregulation of HO-1 (coordinated via the Nrf2-SLC7A11-HO-1 hierarchy) and ferrous ion accumulation. The mechanistic findings encouraged us to rationally apply targeted strategy against HO-1 upregulation and ferrous ion accumulation. The potent strategy by inhibiting HO-1 overexpression was employed to prevent RPE ferroptosis and subsequently photoreceptor degeneration. We found that HO-1 knockdown or HO-1 inhibitor ZnPP can inhibit RPE ferroptosis through the disruption of the vicious loop between ferrous ion accumulation and upregulation of HO-1, eventually preventing photoreceptor degeneration and protecting the visual functionalities. Owing to its targeted HO-1-mediated ferroptotic RPE therapy, inhibiting HO-1 overexpression is highly promising for the treatment of RPE ferroptosis-related diseases in future clinical therapy.

4. Methods and materials

4.1. Materials

NaIO₃, Erastin, DMSO, malondialdehyde (MDA) assay kit, C11-BODIPY (581/591) and fluorescein isothiocyanate (FITC)-dextran (4 kDa) were obtained from Sigma-Aldrich. Ferroptosis inhibitors (Fer-1 and DFO), and ferric ammonium citrate (FAC) were purchased from Selleck chemicals (Houston, TX, USA). DMEM/F12 medium, penicillin/streptomycin, fetal bovine serum (FBS), and live/dead kit were purchased from Invitrogen. FerroOrange, cell counting kit-8 (CCK-8) reagent, and GSSG/GSH Quantification Kit were purchased from Dojindo (China Co., Ltd, China). Dihydroethidium (DHE) was obtained from Beyotime Biotechnology. Zinc protoporphyrin-9 (ZnPP) and Hemin were purchased from Cayman Chemicals (Ann Arbor, MI, USA). Other chemicals were purchased from Thermo Scientific (Waltham, MA, USA) unless stated otherwise.

4.2. Cell culture and treatment

Human RPE (ARPE-19) cells were purchased from American Type Culture Collection (ATCC, Manassas, VA, USA) and were further validated using short tandem repeat (STR) analysis by Shanghai Biowing Applied Biotechnology Co. Ltd. Cells were cultured in DMEM/F12 medium supplemented with 100 U/ml penicillin, 100 µg/ml streptomycin and 10% FBS at 37 °C with 5% CO₂ in incubator. Culture medium was changed every 2 days prior to initiating experiments.

For each experiment using cultured ARPE-19 cells, the plating density was 1×10^4 cells well⁻¹ in 96-well plates, 2×10^4 cells well⁻¹ in 24-well plates, 2×10^5 cells well⁻¹ in 6-well plates, and 5×10^5 cells in 6-cm dishes. One day later, ARPE-19 cells were pretreated with Fer-1 (dissolved in DMSO, 10 µM), DFO (dissolved in deionized water, 75 µM), or ZnPP (dissolved in DMSO, 10 µM) for 1 h, followed by treatment with 1X PBS, NaIO₃ (dissolved in 1X PBS, 30 mM), Erastin (dissolved in DMSO, 5 µM) or FAC (dissolved in deionized water, 250 µmol/L) for 24 h. These same plating conditions were used in all experiments unless mentioned otherwise.

4.3. Transmission electron microscopy (TEM)

ARPE-19 cells cultured with NaIO₃ and Erastin for 24 h were collected. Then they were prefixed in 2.5% glutaraldehyde phosphate (0.1 M, pH 7.4) (Science Services) overnight at 4 °C, and postfixed in 2% buffered osmium tetroxide, then embedded in Epon812 (Merck) followed by dehydration. Ultrathin sections (60 nm thick) were cut, and stained with uranyl acetate and lead citrate. Pictures were finally examined by TEM microscopy (FEI, Hillsboro, OR, USA).

4.4. Live/dead staining and CCK-8 analysis

Live/dead and CCK-8 reagents were applied to detect cell viability in

ARPE-19 cells treatment with different inducers with or without the pretreatment of various inhibitors according to recommended procedures. ARPE-19 cells were seeded in 96-well plates and 24-well plates for CCK-8 and live/dead assay, respectively. At determined time, fluorescence microscope (Nikon) was employed to take photos after staining with live/dead kit for 15 min, PI stained for dead cells, and Calcein AM stained for live cells. After incubation of CCK-8 (10 µL well⁻¹) for 4 h, ELISA microplate reader (ELX800, BioTek, USA) was used to detect optical density at 450 nm (O.D. 450 nm). Cell viability was evaluated by calculating the values of O.D. 450 nm as percentage and normalized to control.

4.5. Permeability assay

A triple cell layer model for studying the RPE permeability is established on permeable membrane filters (Transwell; Corning Costar) according to previous report [48], which consists of human ARPE-19 cells, polycarbonate membranes with 0.4 µm pores, and primary human umbilical vein-derived endothelial cells (HUVEC). In this model, human ARPE-19 cells (seeded onto the basolateral side) and HUVEC (apical side) were co-cultured on the filter membrane. Aliquots were collected from the basolateral side after the addition of FITC-dextran (4 kDa, 10 µM) to the apical side. Fluorescence intensity, equivalent to the relative amount of FITC-dextran was quantified using a microplate reader at 485 nm excitation and 528 nm emission. RPE cell permeability was evaluated by calculating the diffusion rate as follows: (amount of dextran in the lower chamber) × 100/(amount of dextran in the upper chamber).

4.6. Phagocytosis assay

Phagocytosis is assessed using pHrodo™ *E. coli* red fluorescent bioparticles (Invitrogen) as previously described [49]. This bioparticles can fluoresce when internalized in the reduced pH environment of intracellular phagosomes, but do not fluoresce at neutral pH [49], thus background fluorescence associated with nonspecific adherence is negligible. Briefly, bioparticles were prepared at the concentration of 5 µg/µL in Live Cell Imaging Solution (Invitrogen). Confluent ARPE-19 cells were incubated with bioparticles in a 24-well plate for 3 h at 37 °C in CO₂-independent medium (Invitrogen). Negative control plates were incubated at 4 °C. Cells were imaged under the fluorescence microscope.

4.7. Detection of intracellular ferrous ions and LOS

Live-cell fluorescent levels of total intracellular ferrous ion and LOS were detected using FerroOrange (10 µM) and C11-BODIPY (581/591) (5 µM), respectively. When cells have been treated with test compounds at the indicated times, Cells in 6-well dishes were re-suspended in 500 ml of fresh Hank's balanced salt solution (HBSS) for C11-BODIPY evaluation for 20 min at 37 °C culture incubator, and cells in 24-well plates were used for FerroOrange staining in HBSS for 30 min at 37 °C. After washing for three times, intracellular FerroOrange fluorescence imaging was taken by a fluorescence microscope. Cells for LOS detection were trained via a 40 µm cell strainer and then detected by flow cytometer (Accuri C6, BD Biosciences) with excitation of 488 nm laser, or measured under a microplate reader (BioTek, Gen5, Winooski, VT, USA). Increased percentages LOS levels were determined by quantitating and calculating the ratio of 488 nm channel intensity in treated groups to that in control groups.

4.8. GSH measurement

Treated RPE cells as indicated were harvested and were lysed by sonication at 0 °C for 20 min followed by centrifugation at 15,000 g at 4 °C for 10 min. Cleared supernatant was prepared for detecting total protein concentration using Protein Assay Kit (Thermo Fisher Scientific), and for measuring the amount of GSH using GSSG/GSH

Quantification Kit. To remove protein from samples prior to GSH measurement, 1/6 volume of 5% 5-sulfosalicylic acid dihydrate (Wako) in distilled water was used. Samples were centrifuged at 15,000 g at 4 °C for 10 min, and the supernatant was used to determine the GSH assay. The protein and GSH levels of the samples were detected according to the instructions of the kit by measuring absorbance at 405 nm using a plate reader. Values for total GSH levels were calculated and corrected by the protein concentration in the same sample and normalized to control.

4.9. RNA extraction and quantitative polymerase chain reaction (qPCR)

Total RNAs of *in vitro* treated-ARPE-19 or *in vivo* mRPE were isolated and extracted, and qPCR was performed as our previous study reported [50]. Briefly, 5×10^5 cells of each group were collected and extracted using TRIzol reagent. cDNAs were reversely transcribed from ribonucleic acid, and real-time qPCR was performed using Real-Time PCR Detection System (Applied Biosystems, Foster, CA) according to manufacturer's instructions. qPCR data were normalized to the internal control gene expression of GAPDH to ensure accurate gene quantification. The genes and their respective parameters were listed in Supporting Table S1.

4.10. Western blot analysis

At determined time, *in vitro* ARPE-19 cells, *in vivo* mRPE and neurosensory retinae (completely dissected away from underlying RPE) were suspended in protein lysis RIPA (Invitrogen) consisting of proteinase inhibitors (Roche). Protein concentrations were measured using protein assay kit of Bio-Rad (Hercules, CA, USA). Lysate proteins then were separated by SDS-PAGE gels and transferred onto PVDF membranes (EMD Millipore). After blocking with 5% BSA, membranes were incubated with different primary antibodies that were listed in Supporting Table S2, and then were reacted with horseradish peroxidase-conjugated secondary anti-rabbit/mouse antibodies (EMD Millipore, 1:5,000). Protein signaling was viewed by ECL Plus Western Blot Detection Kit (Tanon).

4.11. Immunocytochemistry (ICC) analysis

ARPE-19 cells were seeded on sterile coverslips and embedded in 24-well plates. Cells after treatment were fixed with 4% PFA for 30 min and then were blocked with 10% goat serum in PBS. Protein expression levels in cells were measured by reacting with primary antibodies (listed in Supporting Table S3). After that cells were reacted with secondary anti-mouse/rabbit antibodies-conjugated with Alexa Fluor® 488 or 594 (Invitrogen, 1:800), and nucleus were stained with 4, 6 diamidino-2-phenylindole (DAPI, Invitrogen, 1:8000), fluorescence photos were imaged by fluorescence microscope (Nikon).

4.12. RNA-sequencing and analysis

Total RNA extraction of ARPE-19 cells, cDNA library construction, and sequencing were carried out by RNA-sequencing technology at KangChen Bio-tech (Shanghai, China). High-quality reads were aligned to the human reference genome (hg19, Genome Reference Consortium GRCh37) using Hisat2 software (version 2.1.0). Gene level fragments per kilobase of exon per million fragments (FPKM) were mapped and significant changes in gene and transcript expression levels were calculated using Ballgown software (version 2.10.0). Differentially expressed genes were calculated by a cut-off at a $P < 0.05$, and the absolute value of \log_2 (fold change) greater than or equal to 1.

4.13. siRNA and lentiviral transfection

Human ARPE-19 cells were seeded in 6-well plates seeded for 24 h

and transfected with siRNA or lentiviral plasmid as instructed by manufacturer (GenePharma and Genechem). The siRNA sequences used for gene knockdown in this study were listed in Supporting Table S4, and were transiently transfected with cells using Lipofectamine 3,000 transfection reagent (Invitrogen). After transfection for 8 h, medium was refreshed with complete medium and these cells were cultivated for overnight in incubator prior to being re-seeded for experiments.

For the overexpression of HO-1, ARPE-19 cells were transfected with empty lentiviral plasmid (EF-1aF/GFP&Puro), or human HO-1 cDNA-contained lentiviral plasmid in polybrene (5 $\mu\text{g}/\text{ml}$) for 24 h. For the overexpression of SLC7A11, ARPE-19 cells were transfected with empty lentiviral plasmid (CMV-MCS-EF1 α -copGFP-T2A-puro), or human SLC7A11 cDNA-contained lentiviral plasmid in HiTransG P for 16 h. The normal culture medium incubated cells until the end of the estimate.

4.14. Animal treatment

In this study, sixteen-week-old male C57BL/6 mice were used and housed in a standard laboratory environment. All experiments were in accordance with Association for Research in Vision and Ophthalmology Statement and approved by the institutional animal care and committee of Ninth People's Hospital, Shanghai Jiao Tong University School of Medicine. For *in vivo* studies, left eyes were pretreated with a single intravitreal injection of DMSO (1 μL) or 1X PBS (1 μL), and right eyes were pretreated with Fer-1 (30 μM , a single intravitreal injection, 1 μL), DFO (100 μM , a single intravitreal injection, 1 μL), or ZnPP (50 mg/kg, intraperitoneal injection once a week). 15 min later, injection of NaO₃ (35 mg/kg, a single injection via tail vein), or 1X PBS (a single injection via tail vein, 75 μL) has been performed. After 2 weeks, mice were used for subsequent experiments.

Before *in vivo* mRPE detection, eyes were enucleated and neural retinae underlying RPE were carefully isolated. mRPE cells were separated from other structures by enzymatic (hyaluronidase and dispase) digestion at 37 °C for 30 min and mechanical dissection [45]. Cells were further dissociated with 0.25% trypsin-EDTA for 5 min and counted using a hemocytometer.

4.15. MDA level measurement

Lipid peroxidation assay kit was used to detect MDA level according to manufacturer's recommendation (Sigma-Aldrich) [51]. Cells (1×10^6) were collected in 300 μL of MDA lysis buffer containing 3 μL of butylated hydroxytoluene (BHT, reducing the interfering lipid oxidation, $100 \times$) and homogenized on ice. Samples were centrifuged at 13,000 g for 10 min and then the insoluble material were removed. Subsequently, 600 μL of thiobarbituric acid (TBA, reacting with other compounds in samples giving other colored products) solution was added into each experimental sample or vial containing standard sample to form the MDA-TBA adduct, which were then incubated for 60 min at 95 °C. Followed by cooling to 25 °C in ice bath, 200 μL of each reaction mixture was pipetted into 96-well plates for colorimetric assays to measure the absorbance at 532 nm.

4.16. Haematoxylin and eosin (H&E) and immunofluorescence (IF)

At determined time, mice eyes were separated, and fixed in 10% PFA and embedded in paraffin followed by dehydrated using a series of ethanol solutions. Retinal sections with 6 μm -thick were evaluated by H&E or IF staining. As described previously [52], retinal sections and RPE flat mounts were blocked in buffer containing 5% goat serum in PBS with or without 0.1% Triton X-100. Subsequently, samples were incubated with primary antibodies (listed in Supporting Table S3) for 8 h at 4 °C. Removing primary antibodies, alexa fluor 488/594-conjugated secondary anti-mouse/rabbit antibodies (1:500, Invitrogen) were added to incubate for 1 h at 37 °C. Nuclei were stained with DAPI (Invitrogen). Images were taken through a microscope (Nikon).

4.17. DHE staining

The oxidative fluorescent dye DHE (Beyotime Biotechnology) was used to measure total ROS levels in fresh eye sections according to previously described method [53]. Briefly, intracardial injection of 20 ml of 10 μ M DHE into treated mice. Then the eyes were immediately disassociated for serial sections and then were incubated with DAPI for 30 min at 37 °C, followed by microscopy detection.

4.18. Fluorescein angiography (FA)

FA was performed for the visualization of retinal vasculature. Mice were anesthetized at day 14 after treatment and placed on a custom-made platform positioned on the chin rest of Heidelberg Spectralis device (Heidelberg Engineering GmbH, Heidelberg, Germany). Hydroxypropylmethylcellulose (Methocel 2%; OmniVision, Neuhausen, Switzerland) was used to keep the cornea hydrated of each eye during imaging. 50 μ L of fluorescein sodium (10%, Alcon, China) were injected intraperitoneally, then FA fundus images were acquired.

4.19. Electroretinography (ERG)

Full field ERG was performed as previous study described [54]. After 2 weeks' treatments, mice with dark adaptation overnight were prepared under red light after being anesthetized, and eyes were dilated. Reference and ground electrodes were hooked in forehead and tail, respectively. Espion E3 machine (Diagnosys, Boxborough, MA) was used to record the responses of rods to light stimulants from a pair of 3 mm gold loop electrodes placed on cornea. A single flash stimulus was performed at an intensity of 10 cd s/m² to elicit scotopic ERGs. The a-wave amplitude was measured from the baseline wave to the trough of the first negative wave, and b-wave amplitude was measured from the baseline wave to the peak of the first positive wave or, if the a-wave was presented, from the trough of the a-wave to the peak of the first positive wave. All ERG were carried out at the same time of day.

4.20. Statistical analysis

Statistics were presented as mean \pm standard deviation (SD) from at least 3 repeated experiments (n = 3) unless otherwise described. Values of experimental data were analyzed by unpaired two-tailed Student t-test to compare two groups, and one-way analysis of Variance (ANOVA) for multiple comparison with Bonferroni correction. P<0.05 was considered to be statistically significant.

Availability of data

The raw RNA-sequencing data reported in this study have been deposited in the Gene Expression Omnibus database with the accession number GSE142591, and are publicly accessible at <https://www.ncbi.nlm.nih.gov/geo/query/acc.cgi?acc=GSE142591>.

Author contributions

P. G.: conception and design, revision and approve of the manuscript; J. Z.: conception of the manuscript; Z. T., Y. J., and X. D.: performing research, and drafting the article; N. N., Y. L., and D. Z.: performing research and revising the article; H. G.: acquisition of data; H. S.: analysis and interpretation of data. Z. T., Y. J., and X. D.: contributed equally to this work.

Declaration of competing interest

The authors declare that they have no conflict of interest.

Acknowledgements

This work was supported by National Natural Science Foundations of China (81870687, 82071004), National Key R&D program of China (2018YFC1106100), Key program of Shanghai Science and Technology Commission (19JC1415503), Municipal Education Commission-Gaofeng Clinical Medicine Grant Support (20161316), and Science and Technology Commission of Shanghai (17DZ2260100).

Appendix A. Supplementary data

Supplementary data to this article can be found online at <https://doi.org/10.1016/j.redox.2021.101971>.

References

- [1] P.T. de Jong, Age-related macular degeneration, *N. Engl. J. Med.* 355 (14) (2006) 1474–1485.
- [2] S.R. Flaxman, R.R.A. Bourne, S. Resnikoff, P. Ackland, T. Braithwaite, M. V. Cicinelli, et al., Global causes of blindness and distance vision impairment 1990–2020: a systematic review and meta-analysis, *Lancet Glob. Health.* 5 (12) (2017) e1221–e1234.
- [3] A.P. Voigt, K. Mulfaul, N.K. Mullin, M.J. Flamme-Wiese, J.C. Giacalone, E. M. Stone, et al., Single-cell transcriptomics of the human retinal pigment epithelium and choroid in health and macular degeneration, *Proc. Natl. Acad. Sci. U. S. A.* 116 (48) (2019) 24100–24107.
- [4] W.L. Wong, X. Su, X. Li, C.M. Cheung, R. Klein, C.Y. Cheng, et al., Global prevalence of age-related macular degeneration and disease burden projection for 2020 and 2040: a systematic review and meta-analysis, *Lancet Glob. Health.* 2 (2) (2014) e106–e116.
- [5] A. Biesemeier, E. Voeruek, O. Eibl, U. Schraermeyer, Iron accumulation in Bruch's membrane and melanosomes of donor eyes with age-related macular degeneration, *Exp. Eye Res.* 137 (2015) 39–49.
- [6] T. Ito, M. Nakano, Y. Yamamoto, T. Hiramitsu, Y. Mizuno, Hemoglobin-induced lipid peroxidation in the retina: a possible mechanism for macular degeneration, *Arch. Biochem. Biophys.* 316 (2) (1995) 864–872.
- [7] O. Vergara, T. Ogden, S. Ryan, Posterior penetrating injury in the rabbit eye: effect of blood and ferrous ions, *Exp. Eye Res.* 49 (6) (1989) 1115–1126.
- [8] J. Hanus, C. Anderson, S. Wang, RPE necroptosis in response to oxidative stress and in AMD, *Ageing Res. Rev.* 24 (Pt B) (2015) 286–298.
- [9] A.U. Sapkal, S. Nashine, S. Mansoor, V.R. Sharma, C.A. Ramirez, R.Z. Migon, et al., Protective Effects of 17beta-Estradiol on Benzo(e) pyrene[B(e)P]-induced Toxicity in ARPE-19 cells, *Ageing Res. Rev.* 13 (4) (2018) 419–425.
- [10] S.K. Mitter, C. Song, X. Qi, H. Mao, H. Rao, D. Akin, et al., Dysregulated autophagy in the RPE is associated with increased susceptibility to oxidative stress and AMD, *Autophagy* 10 (11) (2014) 1989–2005.
- [11] K.H. Jang, Y.J. Do, D. Son, E. Son, J.S. Choi, E. Kim, AIF-independent parthanatos in the pathogenesis of dry age-related macular degeneration, *Cell Death Dis.* 8 (1) (2017), e2526.
- [12] A. Southon, K. Zostak, K.M. Acevedo, K.A. Dent, I. Volitakis, A.A. Belaidi, et al., Cu (II) (atSm) inhibits ferroptosis: implications for treatment of neurodegenerative disease, *Br. J. Pharmacol.* 177 (3) (2020) 656–667.
- [13] J.J. Lee, K. Ishihara, S. Notomi, N.E. Efstathiou, T. Ueta, D. Maidana, et al., Lysosome-associated membrane protein-2 deficiency increases the risk of reactive oxygen species-induced ferroptosis in retinal pigment epithelial cells, *Biochem. Biophys. Res. Commun.* 521 (2) (2020) 414–419.
- [14] W. Shu, B.H. Baumann, Y. Song, Y. Liu, X. Wu, J.L. Dunaief, Ferrous but not ferric iron sulfate kills photoreceptors and induces photoreceptor-dependent RPE autofluorescence, *Redox Biol.* (2020), 101469.
- [15] Y. Sun, Y. Zheng, C. Wang, Y. Liu, Glutathione depletion induces ferroptosis, autophagy, and premature cell senescence in retinal pigment epithelial cells, *Cell Death Dis.* 9 (7) (2018) 753.
- [16] M.E. Pennesi, M. Neuringer, R.J. Courtney, Animal models of age related macular degeneration, *Mol. Aspect. Med.* 33 (4) (2012) 487–509.
- [17] H. Schipper, W. Song, H. Zukor, J. Hascalovici, D. Zeligman, Heme oxygenase-1 and neurodegeneration: expanding frontiers of engagement, *J. Neurochem.* 110 (2) (2009) 469–485.
- [18] A. Ahmad, H. Zhuang, S. Doré, Heme oxygenase-1 protects brain from acute excitotoxicity, *Neuroscience* 141 (4) (2006) 1703–1708.
- [19] Y. Yuan, J. Guo, Q. Zhou, The homeostasis of iron and suppression of HO-1 involved in the protective effects of nimodipine on neurodegeneration induced by aluminum overloading in mice, *Eur. J. Pharmacol.* 586 (2008) 100–105.
- [20] M. Catanzaro, C. Lanni, F. Basagni, M. Rosini, S. Govoni, M. Amadio, Eye-light on age-related macular degeneration: targeting nrf2-pathway as a novel therapeutic strategy for retinal pigment epithelium, *Front. Pharmacol.* 11 (844) (2020).
- [21] Castilho Á, C.A. Avelaira, E.C. Leal, N.F. Simões, C.R. Fernandes, R.I. Meirinhos, et al., Heme oxygenase-1 protects retinal endothelial cells against high glucose- and oxidative/nitrosative stress-induced toxicity, *PLoS One* 7 (8) (2012), e42428.
- [22] X. Fang, H. Wang, D. Han, E. Xie, X. Yang, J. Wei, et al., Ferroptosis as a target for protection against cardiomyopathy, *Proc. Natl. Acad. Sci. U. S. A.* 116 (7) (2019) 2672–2680.

- [23] O. Adedoyin, R. Boddu, A. Traylor, J.M. Lever, S. Bolisetty, J.F. George, et al., Heme oxygenase-1 mitigates ferroptosis in renal proximal tubule cells, *Am. J. Physiol. Ren. Physiol.* 314 (5) (2018), F702–f14.
- [24] B.R. Stockwell, X. Jiang, W. Gu, Emerging mechanisms and disease relevance of ferroptosis, *Trends Cell Biol.* 30 (6) (2020) 478–490.
- [25] K. Totsuka, T. Ueta, T. Uchida, M.F. Roggia, S. Nakagawa, D.G. Vavvas, et al., Oxidative stress induces ferroptotic cell death in retinal pigment epithelial cells, *Exp. Eye Res.* 181 (2019) 316–324.
- [26] M.Y. Kwon, E. Park, S.J. Lee, S.W. Chung, Heme oxygenase-1 accelerates erastin-induced ferroptotic cell death, *Oncotarget* 6 (27) (2015) 24393–24403.
- [27] J.W. Kim, K.H. Kang, P. Burrola, T.W. Mak, G. Lemke, Retinal degeneration triggered by inactivation of PTEN in the retinal pigment epithelium, *Genes Dev.* 22 (22) (2008) 3147–3157.
- [28] J. Wang, J. Iacovelli, C. Spencer, M. Saint-Geniez, Direct effect of sodium iodate on neurosensory retina, *Invest. Ophthalmol. Vis. Sci.* 55 (3) (2014) 1941–1953.
- [29] S.J. Dixon, K.M. Lemberg, M.R. Lamprecht, R. Skouta, E.M. Zaitsev, C.E. Gleason, et al., Ferroptosis: an iron-dependent form of nonapoptotic cell death, *Cell* 149 (5) (2012) 1060–1072.
- [30] K. Ueda, H.J. Kim, J. Zhao, Y. Song, J.L. Dunaief, J.R. Sparrow, Iron promotes oxidative cell death caused by bisretinoids of retina, *Proc. Natl. Acad. Sci. U. S. A.* 115 (19) (2018) 4963–4968.
- [31] L. Pedrera, R.A. Espiritu, U. Ros, J. Weber, A. Schmitt, J. Strohm, et al., Ferroptotic pores induce Ca²⁺ fluxes and ESCRT-III activation to modulate cell death kinetics, *Cell Death Differ.* (2020), <https://doi.org/10.1038/s41418-020-00691-x>.
- [32] B. Hassannia, P. Vandenabeele, T. Vanden Berghe, Targeting ferroptosis to iron out cancer, *Canc. Cell* 35 (6) (2019) 830–849.
- [33] H. Wang, P. An, E. Xie, Q. Wu, X. Fang, H. Gao, et al., Characterization of ferroptosis in murine models of hemochromatosis, *Hepatology* 66 (2) (2017) 449–465.
- [34] W.S. Yang, R. SriRamaratnam, M.E. Welsch, K. Shimada, R. Skouta, V. S. Viswanathan, et al., Regulation of ferroptotic cancer cell death by GPX4, *Cell* 156 (1–2) (2014) 317–331.
- [35] L.C. Chang, S.K. Chiang, S.E. Chen, Y.L. Yu, R.H. Chou, W.C. Chang, Heme oxygenase-1 mediates BAY 11-7085 induced ferroptosis, *Canc. Lett.* 416 (2018) 124–137.
- [36] S.J. Dixon, D.N. Patel, M. Welsch, R. Skouta, E.D. Lee, M. Hayano, et al., Pharmacological inhibition of cystine-glutamate exchange induces endoplasmic reticulum stress and ferroptosis, *eLife* 3 (2014), e02523.
- [37] B. Hassannia, B. Wiernicki, I. Ingold, F. Qu, S. Van Herck, Y.Y. Tyurina, et al., Nano-targeted induction of dual ferroptotic mechanisms eradicates high-risk neuroblastoma, *J. Clin. Invest.* 128 (8) (2018) 3341–3355.
- [38] M.M. Gaschler, A.A. Andia, H. Liu, J.M. Csuka, B. Hurlocker, C.A. Vaiana, et al., FINO(2) initiates ferroptosis through GPX4 inactivation and iron oxidation, *Nat. Chem. Biol.* 14 (5) (2018) 507–515.
- [39] X. Yu, N. Song, X. Guo, H. Jiang, H. Zhang, J. Xie, Differences in vulnerability of neurons and astrocytes to heme oxygenase-1 modulation: implications for mitochondrial ferritin, *Sci. Rep.* 6 (2016) 24200.
- [40] H. Chen, X. Wang, Q. Zhao, Z. Zhang, X. Ye, F. Hua, et al., Dual effects of heme oxygenase-1 on astrocyte injury induced by hemin in vitro, *Brain Inj.* 30 (1) (2016) 36–42.
- [41] W. Song, H. Zukor, S. Lin, J. Hascaloivici, A. Liberman, A. Tavittian, et al., Schizophrenia-like features in transgenic mice overexpressing human HO-1 in the astrocytic compartment, *J. Neurosci.* 32 (32) (2012) 10841–10853.
- [42] M. Rossi, S. Delbaue, E. Wespes, T. Roumeguère, O. Leo, V. Flamand, et al., Dual effect of hemin on renal ischemia-reperfusion injury, *Biochem. Biophys. Res. Commun.* 503 (4) (2018) 2820–2825.
- [43] A. Daruich, Q. Le Rouzic, L. Jonet, M.C. Naud, L. Kowalczyk, J.A. Pournaras, et al., Iron is neurotoxic in retinal detachment and transferrin confers neuroprotection, *Sci. Adv.* 5 (1) (2019), eaau9940.
- [44] D. Nowis, M. Bugajski, M. Winiarska, J. Bil, A. Szokalska, P. Salwa, et al., Zinc protoporphyrin IX, a heme oxygenase-1 inhibitor, demonstrates potent antitumor effects but is unable to potentiate antitumor effects of chemotherapeutics in mice, *BMC Canc.* 8 (2008) 197.
- [45] C. Zhao, D. Yasumura, X. Li, M. Matthes, M. Lloyd, G. Nielsen, et al., mTOR-mediated dedifferentiation of the retinal pigment epithelium initiates photoreceptor degeneration in mice, *J. Clin. Invest.* 121 (1) (2011) 369–383.
- [46] Y. Saito, Y. Kuse, Y. Inoue, S. Nakamura, H. Hara, M. Shimazawa, Transient acceleration of autophagic degradation by pharmacological Nrf2 activation is important for retinal pigment epithelium cell survival, *Redox Biol.* 19 (2018) 354–363.
- [47] D. Kokona, A. Ebnetter, P. Escher, M. Zinkernagel, Colony-stimulating factor 1 receptor inhibition prevents disruption of the blood-retina barrier during chronic inflammation, *J. Neuroinflammation* 15 (1) (2018) 340.
- [48] Q. Jiang, C. Liu, C.P. Li, S.S. Xu, M.D. Yao, H.M. Ge, et al., Circular RNA-ZNF532 regulates diabetes-induced retinal pericyte degeneration and vascular dysfunction, *J. Clin. Invest.* 130 (7) (2020) 3833–3847.
- [49] C.H. Peng, J.H. Chuang, M.L. Wang, Y.Y. Jhan, K.H. Chien, Y.C. Chung, et al., Laminin modification subretinal bio-scaffold remodels retinal pigment epithelium-driven microenvironment in vitro and in vivo, *Oncotarget* 7 (40) (2016) 64631–64648.
- [50] Z. Tang, F. Jiang, Y. Zhang, Y. Zhang, YuanYang, X. Huang, et al., Mussel-inspired injectable hydrogel and its counterpart for actuating proliferation and neuronal differentiation of retinal progenitor cells, *Biomaterials* 194 (2019) 57–72.
- [51] S.K. NaveenKumar, B.N. SharathBabu, M. Hemshekhar, K. Kemparaju, K.S. Girish, G. Mugesh, The role of reactive oxygen species and ferroptosis in heme-mediated activation of human platelets, *ACS Chem. Biol.* 13 (8) (2018) 1996–2002.
- [52] D.J. Strick, W. Feng, D. Vollrath, MERTK drives myosin II redistribution during retinal pigment epithelial phagocytosis, *Invest. Ophthalmol. Vis. Sci.* 50 (5) (2009) 2427–2435.
- [53] R. Mohamed, I. Sharma, A.S. Ibrahim, H. Saleh, N.M. Elsherbiny, S. Fulzele, et al., Hyperhomocysteinemia alters retinal endothelial cells barrier function and angiogenic potential via activation of oxidative stress, *Sci. Rep.* 7 (1) (2017) 11952.
- [54] J. Chen, S. Patil, S. Seal, J.F. McGinnis, Rare earth nanoparticles prevent retinal degeneration induced by intracellular peroxides, *Nat. Nanotechnol.* 1 (2) (2006) 142–150.